Journal of Applied Fluid Mechanics, Vol. 10, No. 5, pp. 1475-1486, 2017.
Available online at www.jafmonline.net, ISSN 1735-3572, EISSN 1735-3645.
DOI: 10.18869/acadpub.jafm.73.242.27617

A Novel Method for Defining the Leeward Edge of the Planar Jet in Crossflow

K. Zhao[1,2], X. Yang[2†], P. N. Okolo[1,3], Z. Wu[2], W. Zhang[2] and G. J. Bennett[1]

[1] *Department of Mechanical and Manufacturing Engineering, Trinity College Dublin, University of Dublin, Dublin, Republic of Ireland*
[2] *College of Aerospace Science and Engineering, National University of Defence Technology, Changsha 410073, P. R.China*
[3] *Energy and Power Technology Division, Department of Mechanical Engineering, University of Nigeria, Nsukka, Nigeria*

†*Corresponding Author Email: nkyangxixiang@163.com*

(Received January 19, 2017; accepted May 8, 2017)

ABSTRACT

To avoid the complexity of the edge definition by the half width, a new approach to defining the leeward edge of the planar jet in crossflow is introduced in this paper. Particle Image Velocimetry (PIV) experiments were performed to measure different flow regimes within the single jet and the dual jets configurations in crossflow. Based on the experimental data acquired, a series of velocity profiles were extracted from the flow field. In each profile, a velocity threshold was given to distinguish the regions sheltered and the regions not sheltered by the planar jet. The boundary of these regions was accordingly recognized as the leeward edge. Furthermore, fitting of the edge was carried out using a second order polynomial so as to enable a mathematical expression of the leeward edge. An application of the proposed approach towards the flow induced noise reduction using a planar jet is also discussed in this paper. In addition, the PIV frame assembly algorithm used in this study is reported.

Keywords: Planar jet; Crossflow; Leeward edge; PIV; Flow-induced noise reduction.

NOMENCLATURE

D	diameter of the tandem cylinders	U_{j1}	speed of the primary planar jet in the single jet configuration and the dual jet configuration
P	pitch of the tandem cylinders	U_m	maximum speed of the local section in the 2D natural system
U_∞	speed of the crossflow		
U_{j2}	speed of the upstream jet in the dual jets configuration		

1. INTRODUCTION

The turbulent jet in crossflow is a fluid problem related to many engineering problems, such as internal cooling of turbine blades, wast water discharge into the costal water, etc. Compared with the round jets, the planar jet in crossflow (PJIC) has attracted less attention due to the limited applications. Recent studies by Oerlemans and Bruin (2009), Zhao *et al*. (2017) have shown the suitability of PJIC towards the reduction of flow-induced noise. The application is foreseen to be the landing gear noise reduction (Sijpkes and Wickerhoff 2004). The basic idea is to insert a planar jet upstream to a bluff body in order to deflect the crossflow. The bluff body is targeted to be situated below the planar jet. This enables the local flow speed to be significantly reduced, thereby reducing the aerodynamic noise. To optimise the configuration so as to achieve the maximum noise reduction, the bluff body position is referred to the leeward edge of the planar jet. Therefore, a crucial defining of the leeward edge is necessary.

In the study of the turbulent jet ejected in a quiescent flow, e.g. the planar jet and the round jet, the edge has been well discussed. Conventionally, the half jet width is utilised to describe the spreading of the turbulent jet. To be more specific, the half jet width represents a typical length where the velocity is equal to half of the trajectory velocity (Rajaratnam 1976). The trajectory velocity is also the maximum velocity

in the local normal plane of the jet trajectory. In the quiescent flow, the jet trajectory can be easily tracked because it is coincident with the geometric centreline. As such, the half width edge can be identified by extracting velocity profiles in the spanwise plane. Furthermore, it is found that the spreading rate (or growth rate) of the jet half width can be expressed as a linear expression depending on the jet centreline axis (Kotsovinos 1976; Ramaprian and Chandrasekhara 1985).

When the turbulent jet is ejected into a crossflow, it bends over downstream due to the entrainment of ambient fluid with crossflow momentum. Then the jet merges with the crossflow and consequently a new mainstream is formed (Rudman 1996; Morton and Ibbetson 1996). In addition, if there exists multiple jets, e.g, in a tandem configuration, the bending curvature of each jet varies due to the shelter from front jets (Lin and Sheu 1991; Tanaka 1974; Yu, Ali, and Lee). Likewise, the jet half width has been applied in the research of PJIC (Haniu and Ramaprian 1989; Smith and Mungal 1998; Persen, iann, and Mazumdar 1993). To begin with, a 2D natural system in PJIC is established. As shown in Fig.1, the 2D system possess 2 axes, denoted as α and β. α is the trajectory of the jet. After α is defined, the normal plane of α, termed as local section hereinafter, can be determined. In the 2D system, β is coincident with the local section. As such, the trajectory definition underlies the establishment of the natural system. To date there are different approaches in the jet trajectory definition: locus of velocity maxima, scalar concentration maxima or vorticity maxima in the local sections. Alternatively, the time-averaged streamline originating at the jet exit can be used as the jet trajectory (Mahesh 2013).

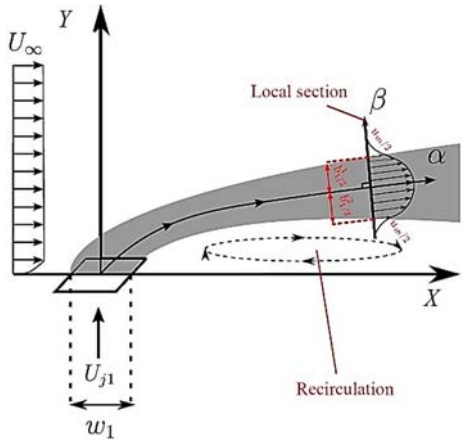

Fig. 1. 2D Natural system in PIC.

When the natural system is established, the half jet width can be introduced. More specifically, as shown in Fig.1, the edges are the locus of those points that possess a velocity of half local maximum (um/2) in the local sections. b11/2 and b21/2 represent the windward and the leeward half width edges of the jet respectively. Research work by Haniu and Ramaprian (1989) achieved the best model to date for the planar jet trajectory prediction. To be more specific, in the absence of significant buoyancy effects, an assumption was made that behaviour of the jet only depends on its initial (kinematic) momentum flux and the crossflow velocity. Therefore, a dimensionless analysis of the relevant variables can be conducted, which yields:

$$\frac{y}{l_m} \propto \left(\frac{x}{l_m}\right)^{\frac{1}{2}} \tag{1}$$

where lm is the momentum length scale for 2D jet, expressed as $l_m = w_1 U^2 / U^2_{j1}$. w1 is width of the jet slot. Based on the experiment data, Eq. 1 was

corrected and the model is written as:

$$\frac{y}{l_m} = 1.2\left(\frac{x}{l_m}\right)^{0.54} \tag{2}$$

More importantly, compared to the measurement from the same jet in quiescent flow (Ramaprian and Chandrasekhara 1985), Haniu and Ramaprian (1989) concluded that the spreading rate of the PJIC is slightly higher. Since the spreading rate in quiescent flow has been well modelled, the conclusion makes it possible to predict the half width edge of the jet to some extent. It is this prediction that is used in the work by Oerlemans and Bruin (2009) to determine the optimised position for the bluff body noise reduction using a planar jet.

However, there are some limitations in the half width edge, which are worth discussing. Firstly, on the edge definition. All definitions of the jet edge are based on the local section. The local section is achieved as the normal plane to the jet trajectory. Meanwhile, the jet trajectory is defined by the locus of the maxima in the local section. As such, there is a suspect of the circular definition. As mentioned above, there are different definitions of the jet trajectory. When the trajectory is defined as the time-averaged streamline that originates from the centre of the jet outlet, the circular definition can be broken up. This is because the streamlines are calculated as those curves that are tangent to the flow velocity field. Even so, another limitation may come out that the local velocity maxima is not situated on the trajectory. Secondly, on the model. Experimental work conducted by Haniu and Ramaprian (1989) utilised a water jet in a water flume, both of which had extremely low speed (Uj1 = 0.3m/s and U∞=0.3m/s, 0.33m/s, and 0.5m/s). Therefore, it necessitates more investigations when the jet speed is much higher. One recent study by Bennett *et al*. (2016) has found the model can well capture the jet trajectory close to the outlet, but being a quadratic curve, the model cannot capture the jet further downstream. At last but not least, on the application. As mentioned above, the model has been applied for bluff body noise reduction. Therefore, the bluff body was situated below the leeward half width edge of the jet. It suggests that the impinging flow speed to the bluff body can be up to half of the local maximum. Reduction of the impinging speed to the bluff body is the key to the noise reduction using the air curtain, concluded by Oerlemans and Bruin (2009) and Zhao *et al*. (2016). Half of the local maximum, to some extent, is still high. Therefore, a more reasonable definition of the leeward edge of the PJIC, especially for noise reduction, is highly expected.

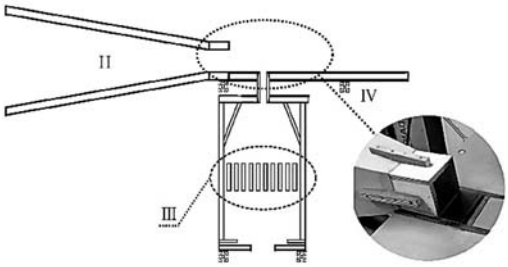

Fig. 2. Schematic of the experimental rig (not in scale): I. microphone array; II. crossflow nozzle; III. honeycomb layer in the jet plenum; IV. endplate and its supporting aluminium extrusion.

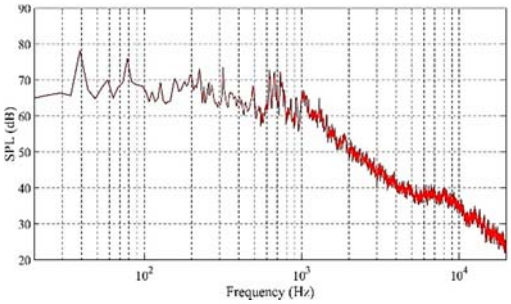

Fig. 3. Auto-spectrum of the wind tunnel background noise.

In this paper, a novel method for defining the leeward edge of the PJIC is proposed based on PIV experiments, which can be used for the single jet and the dual jets configurations in crossflow. Firstly, the experimental facilities and instruments are introduced. Then the proposed method is described in a step-by-step process and the validation is conducted with a series of experimental cases. The corresponding application towards the flow-induced noise reduction is reported. In addition, the PIV frame assembly approach used in this study is introduced.

2. EXPERIMENTAL SETUP AND MODELS

All experiments were conducted in a low speed 3/4 open-jet wind tunnel with a planar jet system. Schematic of the entire rig is shown in Fig.2. In addition, the tandem cylinders were selected as the test body to generate the flow induced noise source. Specifics of the experimental set-up are described in this section.

2.1 Open-Jet Wind Tunnel

The 3/4 openjet wind tunnel was powered by a 5.5 kW centrifugal blower. The dimension of the nozzle (Fig.2.II) is 1000mm long with an outlet size of 75mm×75mm. The outlet was mounted to be flush with a horizontal end-plate. The crossflow coming from the wind tunnel has been characterised by a series of comprehensive measurement using Dantec hot-wire anemometry in the work by Zhao *et al*. (2016). The crossflow speed from the wind tunnel can be up to 70m/s and the free stream turbulence intensity is within 2% in the measurement window. The acoustic performance of the wind tunnel was also characterised using the microphone array introduced in the following section. The auto-spectrum of the background noise when U_∞ = 50.45m/s is shown in Fig.3. It is found that the background noise mainly concentrates in the frequency range that is less than 1,000Hz and SPL dramatically declines when the frequency is higher than 1,000Hz. Therefore, the acoustic analysis in the reminder of the paper will mainly focus on the frequency range over 1,000Hz.

2.2 Planar Jet System

The planar jet system was operated by a 2.2 kW centrifugal blower and a cubic plenum equipped with jet nozzles. The blower was situated to be far from the rig but a hose was between the blower and the plenum, which helps to reduce the background noise. The Plenum was 540 mm high with a horizontal section of 424mm×424mm. One honeycomb layer with the hexagonal grid of 6 mm edge length (Fig. 2. III) was installed inside to uncouple the jet flow from the blower. Baffles were installed to minimise recirculation inside. All internal structures of the plenum were designed to ensure low turbulence intensity in the planar jet.

The number of the jet nozzles could be controlled to be either one or two, depending on specific tests. For the dual jets configuration, rectangular outlets were managed parallel to each other. The span-wise length of the jet nozzles were fixed at 100 mm, and the streamwise width could be controlled as required, i.e. 10mm in this study. Therefore, the length/width ratio was not greater than 10, which allows the regime to be treated as 2D flow. In The lip of the jet nozzles was flush with the end-plate. In the single-jet configuration, jet velocity can be easily controlled by managing the area of the blower inlet. Additionally, in the dual jets configuration, since the mass flow was supplied by the same plenum, the speed difference between two jets was achieved by installing a piece of metal mesh plate, with different porosity, between the plenum and the jet nozzle. Examples of the mesh are shown in Fig.4. Prior to experiment, a variety of mesh porosity were tested in attempt to calibrate the jet speed. In the calibration, the jet speed was measured by FCO510 micromanometer supplied by Furness Controls. As such, the velocities anticipated for both jets could be attained.

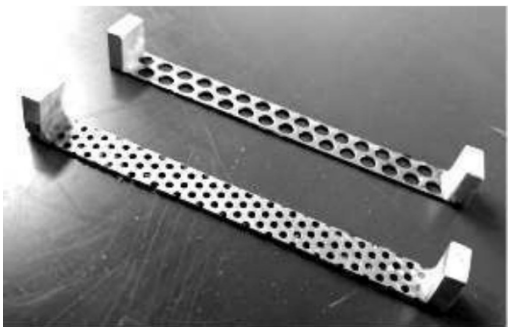

Fig. 4. Examples of the mesh plate inside the planar jet system.

2.3 Test Model

As mentioned earlier, the application of the leeward definition edge definition on the flow induced noise reduction was conducted. In the experimental tests, tandem cylinders were used as the noise source, shown in Fig.5.a. The diameter of the cylinders was 4mm. Previous studies (Zdravkovich 1985; Zdravkovich 1987) concluded that specific values of P/D can lead to different flow regimes. For instance, for intermediate spacing $2.2-2.5 < P/D < 3.1-3.4$ an intermittent shedding can be detected in the region between two cylinders and the vortex shedding mainly occurs on the rear cylinder. These complex flow structures can result in substantial noise production. Therefore, in this study, this regime was selected and P/D was set to be equal to 3. The pitch between two cylinders, P, was 12mm.

Figure 5.b illustrates the setup for the cylinders in the acoustic tests of the single jet configuration. The cylinders were supported by two blocks and the span of the cylinders was much longer than the crossflow width. This avoids the extra noise that is generated if the crossflow blows the block. The relative position of the cylinders is determined referred to the jet leeward edge, which will be reported in the reminder of this paper.

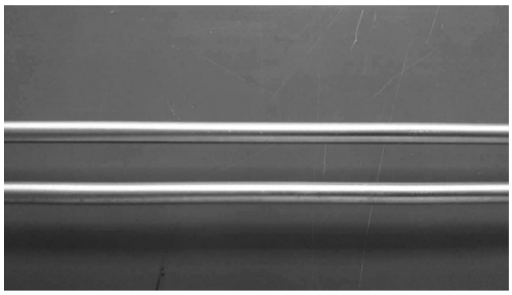

(a)

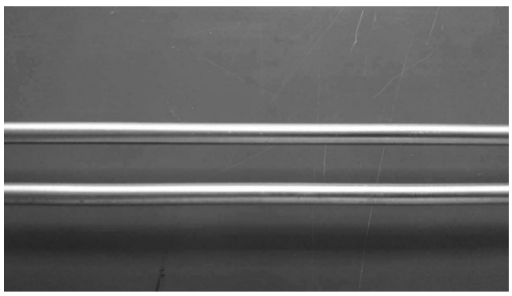

(b)

Fig. 5. Flow induced noise source: (a). tandem cylinders; (b). set-up.

3. EXPERIMENTAL APPARATUS

3.1 PIV

PIV has been widely applied on the studies of jets (in crossflow). For example, work by Camussi *et al*. (2002), Camussi (2002), Kocheb *et al*. (2011), Larsson *et al*. (2012). As previously stated, the leeward edge definition discussed in this study is based on PIV experiment. The arrangement of the PIV measurement is depicted in Fig.6. The instrument was equipped with a LaVision low-speed PIV system with a 15 mJ New Wave Solo-II PIV double pulsed Nd:YAG laser. The laser beam was refocused and diverged by a set of lenses and consequently, a laser sheet could be formed as sharp as 0.3 mm, i.e. the measurement plane. he cross-flow and jets were seeded using Pea Soup Oil Based Smoke Generator PS31. Particle size in all tests were in the range of 1.5μm. Image pairs were recorded using a double exposure LaVision Flow-master 3 camera, with a maximum resolution of 1280×1280 pixels. The camera was attached beside the endplate, which allowed the lens to remain parallel to the laser sheet. Once the camera was focused, it could attain image pairs with a frame size of 97.2 mm×96.9 mm and the time delay between two paired images was 8 μs. However, the streamwise frame length, i.e. lw = 97.2 mm, was not adequate enough to capture the development of the jet. Therefore, the PIV frame assembly was conducted for the time-mean analysis through the Davis software and an open access toolbox in Matlab–PIVMat. More specifically, the Davis software was used to control the PIV instrument, capture and process the pair images. The PIVMat supplied a coding environment in Matlab, in which the post-process and PIV assembly were carried out.

The PIV assembly begins with paired image acquisition. In particular, there are two sampling positions, i.e. C1 and C2 in Fig.6.a. The camera was traversed and respectively situated at C1 and C2. Therefore, two different frames could be achieved, denoted as F1 and F2 and shown in Fig.6.b. It is worth noting that the calibration was only conducted at C1, which means the coordinate system in F1 is correct. However, in F2, the scale of the coordinate system is correct but the origin is not. This problem will be fixed after the assembly. The translation between C1 and C2 is denoted as $lw - \Delta l$, which must be smaller than lw. In this experiment $lw - \Delta l$ was controlled to be 90mm. 400 paired images were acquired at each position respectively. This number of image pairs has been validated to be sufficient to achieve the convergence in the mean quantities, and the time consumption is at a moderate level. The raw data were processed with multi-pass correlation of 32×32 (50%overlap) and 16×16 (25% overlap) in Davis. The file extension of the processed data from Davis is ".vc7", which can be directly loaded in Matlab using the PIVMat for the post-process.

The data loaded for each frame in Matlab, in effect, are stored as the structure array. The core of the array is two matrices and two vectors. These two matrices, with a size of 85 × 107 in this study, contain the velocity components in X and Y respectively. The results were averaged to achieve the time-mean flow field for those two frames. One example is shown in Fig.7 (a) and (b). As the two matrices in each of the two frames possess same structure, they are herein denoted as one capital letter. In other word, one capital letter is used to denote both matrices for X and Y in the same frame. Therefore, and $\bar{B}$ are for the mean field in F1 and F2 respectively, expressed as:

$$\bar{A} = \{a_1, a_2, \dots, a_{\beta-1}, a_\beta\}_{\alpha\times\beta} \tag{3}$$

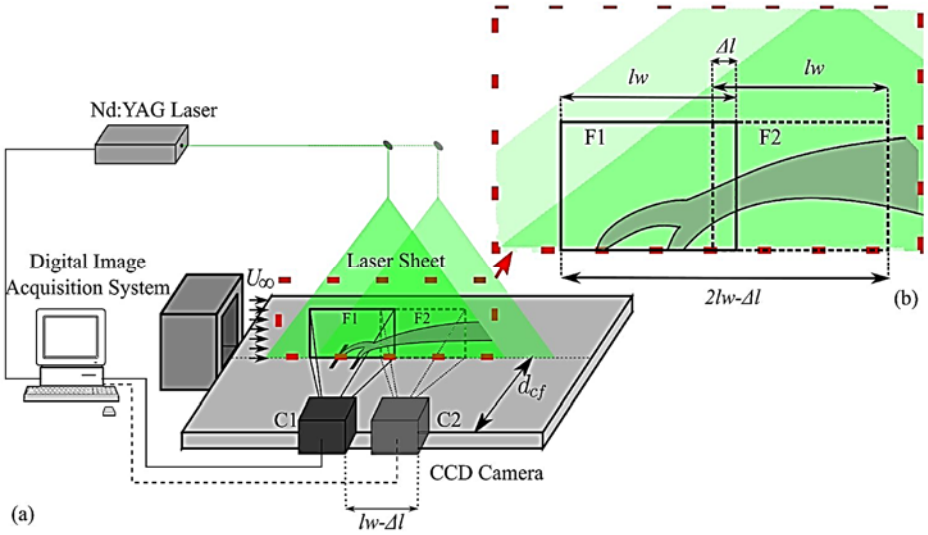

Fig. 6. Schematic of the PIV set-up.

$$\bar{B} = \{b_1, b_2, \dots, b_{\beta-1}, b_\beta\}_{\alpha\times\beta} \quad (4)$$

where α = 85 and β = 107. In the meantime, their corresponding coordinates are provided in the two vectors mentioned above, termed as the coordinate vectors. These two vectors contain the position information in two orthogonal directions, i.e. X and Y. More specifically, 107 elements in X direction and 85 elements in Y direction. Note that after the camera traversed from C1 to C2, the coordinate vectors will not vary with the camera position. Thus, these coordinate vector can be denoted with same symbols in both frames, i.e. Xβ and Yα for X and Y respectively. Elements inside these coordinate vectors are the real X and Y coordinates of each pixel rather than the pixel indices. They can be written as:

$$X_\beta = [x_1, x_2, \dots, x_{\beta-1}, x_\beta] \quad (5)$$

$$Y_\beta = [x_1, x_2, \dots, x_{\alpha-1}, x_\alpha] \quad (6)$$

The number of elements in the streamwise dimension within Δl, i.e. the number of the superposition elements in each frame (n) , is calculated as:

$$n=\left[\beta \times \frac{\Delta l}{l_w}\right] \quad (7)$$

where"[ ]" gives the round integer of the inside value.

The new assembled frame is a combination of F1 and F2 with removing the superposition in F2. Therefore, the length of the new frame is as long as 2lw − Δl and the matrix size for the new assembled frame should be as long as 2β − n. Because the rounding can introduce uncertain error to the assembly. Therefore, a coefficient is introduced for correction, denoted as co. The value of co is dependent on continuity, which can be any of 0, 1, 2, etc. As such, the new assembly is as long as 2β−n+co. is used to term the assembled matrix, written as:

$$\bar{M} = \{a_1, a_2, \dots, a_{\beta-1}, a_\beta, b_{n-co+1}, b_{n-co+2}, \dots, b_{\beta-1}, b_\beta\}_{\alpha\times(\beta-n+\infty)} \quad (8)$$

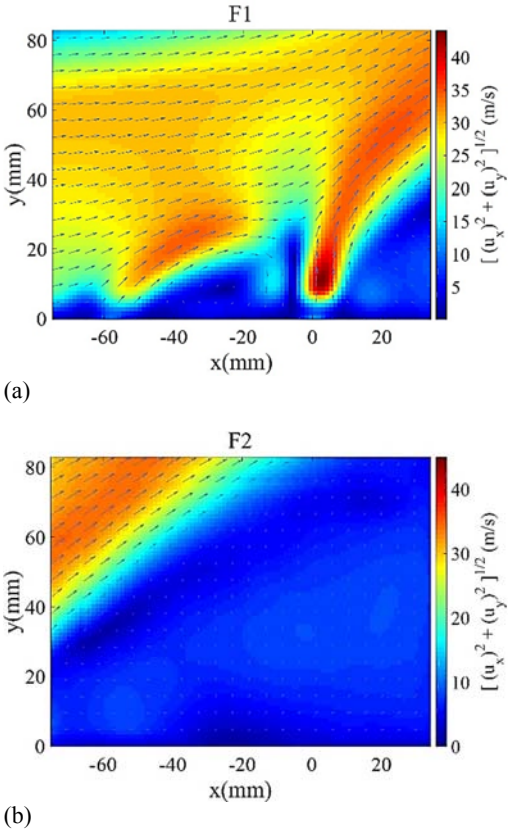

Fig. 7. Example of the time-mean flow field in different frames: (a). F1; (b). F2.

The assembled coordinate vectors for X axis can be written as:

$$X' = \{x_1, x_2, \dots, x_{\beta-1}, x_\beta, x_\beta+\delta, x_\beta+2\delta, \dots, x_\beta+(n-co-1)\delta, x_\beta+(n-co)\delta\}_{1\times(2\beta-n+co)} \quad (9)$$

where δ is the interval between any two adjacent X coordinates in Xβ. Note that δ is a constant once the

calibration has been carried out. Obviously, the assembled coordinate vector for Y remains to be same, i.e.

$$Y' = Y_\alpha \tag{10}$$

Then the assembly array including $\overline{M}$,X' and Y' can be achieved, which can be shown using PIVMat (Fig.8).

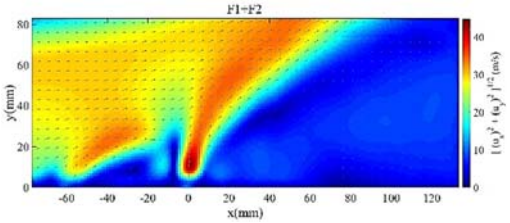

Fig. 8. Example of the assembled frame (F1+F2).

This approach can be of good use when there is limitation of the PIV instrument, e.g. shortage of the camera number. Therefore, it is necessary to discuss the quality of this assembled frame. As an assembly of multiple frames, continuity plays an important role. As mention earlier, the choice of co is subject to continuity. Therefore, the variation of the continuity with co can be a criteria to evaluate the choice of co.

In the continuity analysis in this study, horizontal velocity profiles are used. More specifically, it is known that the joint is somewhere around x = 38.22mm, the uncertainty is attributed to the rounding as well as the choice of co. Therefore, three arbitrary horizontal profiles were extracted, all of which start from x = 30mm and end at x = 40mm. However, those profiles should be averted (c) from being inside the area with high velocity gradient. Therefore, those horizontal profiles with y=18.61mm, y=28.11mm and y=70.88mm were used. These velocity profiles are shown in Fig.9 with different co. The junction inside each subfigure and its adjacent positions have been high-lighted with a rectangle. From the comparison between different co, it is clear shown that the continuity of the speed profile is affected by the value of co. The best continuity for all three profiles occurs when co = 1. Thus, in this study co was set to be equal to one.

3.2 Microphone Array

As mention earlier, the application of the jet lee-ward edge definition on flow-induced noise reduction is described in this paper to show the usefulness of this approach. All acoustic measurements were performed using the microphone array illustrated earlier in Fig. 2.I.

As shown in Fig.10, the array consists of 25KE4 Sennheiser electret microphones. Those microphones worked within 20-20,000Hz range and each of them was equipped with an amplifier to enhance the signal. The distribution of the microphones is illustrated in Fig.11. This irregular pattern was determined using beamforming simulation. A large number of arbitrary pattern was tested using a virtual monopole source, among which the one with the best performance was selected. This pattern also enables to reduce the typical spatial aliasing of the regular one. Data were acquired using National Instrument DAQ system NI PXI-1033. For each test the sampling time and the sampling frequency were 10s and 100kHz. Moreover, one camera was installed in the array, which allowed the noise localization to be based on the real cut-out of the test platform from the top view.

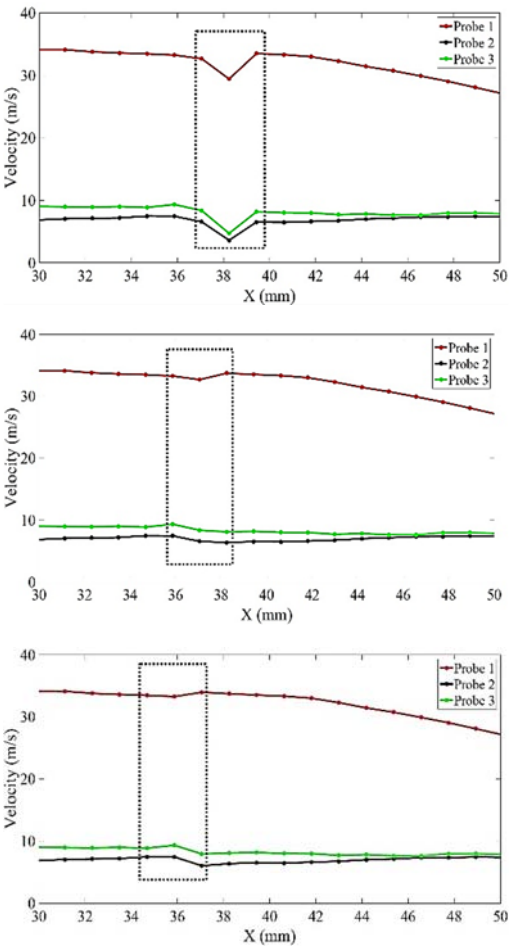

Fig. 9. Continuity analysis of the frame assembly:(a). co = 0; (b). co = 1, (c). co = 2.

Fig. 10. Microphone array.

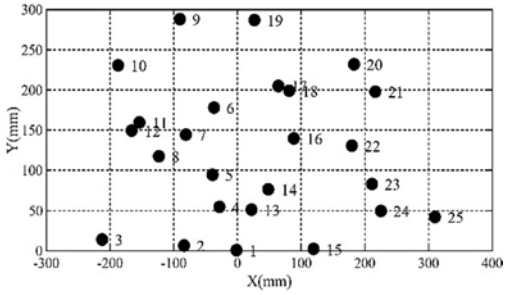

Fig. 11. Arrangement of the microphones in the array.

The acoustic data were processed to achieve overall one third octave band spectra, which are the results as an average of all microphones in the array. Moreover, the conventional beamforming with diagonal deletion was utilised to obtain the noise map. Effects of sound refraction within the wind tunnel shear layer was corrected for, using an Amiet method (Amiet 1978).

4. LEEWARD EDGE DEFINITION

In this section, the process of defining the jet leeward edge is explained in detail.

4.1 Leeward Edge Extraction

The proposal of the method is based on PIV test results. In this study a series of PIV tests with different initial conditions were conducted, reported in Tab.1. The jet speed was measured using FCO510 micromanometer. There are single jet configurations and dual jets configurations. In the dual jets experiment, the distance between centres of the jet slots is 60mm. In addition, each has been distributed a run number.

Table 1 PIV Test matrix of the planar jet in crossflow

No.	U_∞ (m/s)	w_1 (mm)	U_{j1} (m/s)	w_2 (mm)	U_{j2} (m/s)
S1	40.32	10	39.27	/	/
S2	40.12	10	50.15	/	/
S3	29.18	10	41.13	/	/
S4	30.15	10	49.52	/	/
D1	40.35	10	49.15	10	19.98
D2	40.10	10	50.02	10	30.18
D3	40.34	10	49.89	10	49.54
T1	40.56	10	40.45	/	/

Figure12.a shows the mean velocity contour of S1. Note that the X and Y axes have been normalised by the width of the primary jet (w1). A number of vertical probes were extracted to achieve the velocity profile. These profiles were extracted from the mean field of the flow, the one sigma uncertainty of those profiles was found to be within 0.5%. For example, three of these probes, P1, P2 and P3 are illustrated in Fig.12.a and their corresponding velocity profiles are reported in Fig.12.b. From those three profiles, it is observed that P1 and P2 begin with a slow velocity when y/w1 is low. When the height increases, both profiles quickly reach a local maximum, i.e. 17m/s for P1 at y/w1 = 0.3 and 8.5m/s for P2 at y/w1 = 1.2. Subsequently, with y/w1 going higher and having passed the local maximum, the velocity goes slower and then starts to accelerate again until it reaches the global maximum. By contrast, P3 does not display the same trend. It begins with an increase from low velocity and then fluctuates around 10m/s until y/w1 = 3. When the fluctuation ends, the velocity of P3 soars to the maximum. The characteristics of P1, P2 and P3 discussed above can be well explained in the velocity contour. As depicted in Fig.12.a, both P1 and P2 penetrate a relative high speed region below the planar jet. This is the reason why in the profiles of P1 and P2, there is an obvious local maximum when y/w1 is low. However, P3 is always outside the high speed region. Thus, it does not have any obvious reversed trend except increase and fluctuation.

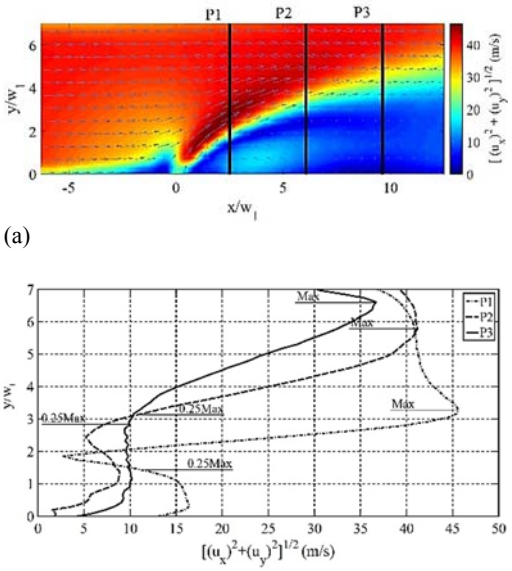

Fig. 12. Velocity profiles extraction (a). examples of the probes (P1, P2 and P3); (b). velocity profiles of P1, P2 and P3.

Formation of the relative high speed region below the jet can be attributed to the recirculation zone induced by the planar jet (Jones and Wille 1996). As schematically shown in Fig.1, a main recirculation zone can be induced below the planar jet due to the entrainment of the ambient fluid. Research on the characterisation of the recirculation structure can be found in previous studies by Pavageau *et al*. (2006), Ahmed *et al*. (2008), etc. However, not much information can be found on how much the recirculation zone affects the bending of the planar jet. The trend of P1, P2 and P3 suggests that characteristics of the velocity profiles are subject to the recirculation zone. Therefore, when the leeward edge is defined, the effects from the recirculation

must be taken into account.

Proceeding further, a speed threshold is proposed. More specifically, the maximum of each velocity profile can be easily localised, marked with 'Max' in Fig.12.b. As discussed earlier, when the planar jet is used for the noise reduction, the bluff body should be situated below the leeward edge, which allows the local flow speed to be reduced. Thus, the leeward edge is the boundary between the low speed region and the high speed region. In other word, the boundary between the sheltered region and the unsheltered region. As such, it is directly related to the velocity profile. A threshold can be used to separate the region sheltered and the region not sheltered by the jet, and the locus of the threshold points in all profiles can be defined as the leeward edge. In this study, an example of the threshold is used, which is equal to one quarter of the maximum velocity. The corresponding location of the threshold points in P1, P2 and P3 are also marked in Fig.12.b. Likewise, more profiles were extracted from the velocity contour and all points with 0.25 maximum velocity are marked and illustrated, which is Fig.13. It is worth noting that in some profiles there are more than one point with 0.25 maximum velocity. These profiles mainly show up in the jet outlet proximity and the very downstream field of this contour window. It suggests that the flow field of these areas are much more complicated than others. A possible explanation can be the recirculation as well, which can result in high velocity gradient in these areas. However, the point with the highest y/w1 in each profile can be easily localised. When all those points are linked, illustrated in Fig.13, a curve will show up, which is the leeward edge.

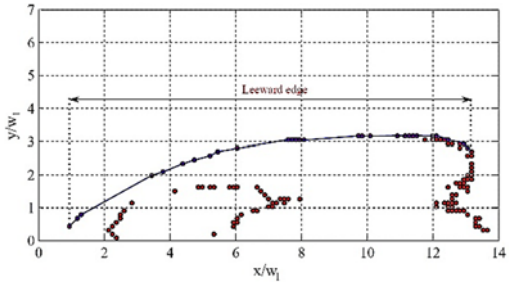

Fig. 13. Threshold points and the leeward edge definition.

4.2 Leeward Edge Fitting

When applied towards the engineering use, the leeward edge frequently requires a mathematical expression. Considering it is characterised by a parabolic shape, a second-order polynomial is attempted to fit the leeward edge, which is written as:

$$\frac{y}{w_1} = f\left(\frac{x}{w_1}\right) = p_0 + p_1\left(\frac{x}{w_1}\right)^1 + p_2\left(\frac{x}{w_1}\right)^2 \qquad (11)$$

The coefficients in Eq.11 are determined by the experimental data. As shown in Fig.14.a, the scatter illustrates data acquired from the PIV experiment. The fitting curves are superimposed on the scatter. Values of the coefficients in the polynomial are reported in Tab. 2. It is observed that the fitting curves are in good agreement with the experimental data, except the point most downstream in S2.

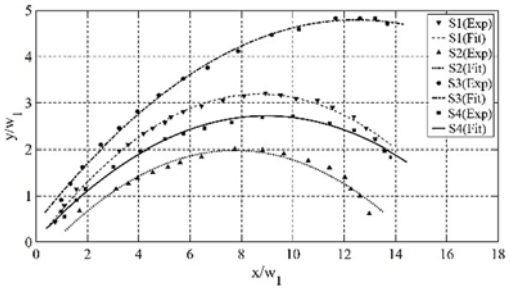

(a)

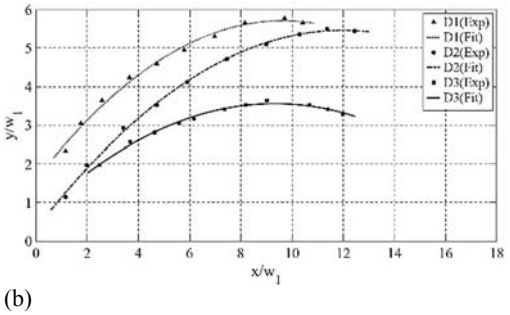

(b)

Fig. 14. Fitting of the primary jet leeward edge:(a). single jet configurations; (b). dual jets configurations.

This point can be eliminated as an abnormal point. Therefore, the error range of the fitting is within 5%difference of y/w1 for each point.

Also, a second-order polynomial was attempted to fit the primary jet leeward edge in the dual jets configurations. Likewise, the comparison between experimental data and fitting curves is depicted in Fig.14.b The good agreement also confirms the efficiency of fitting when applied to the dual jets in cross flow.

Table 2 Coefficients of the second order polynomial for the leeward edge fitting

No.	P_0	P_1	P_1
S1	0.029	0.72	-0.041
S2	-0.456	0.63	-0.041
S3	0.450	0.71	-0.028
S4	0.014	0.61	-0.034
D1	1.6	0.85	-0.044
D2	0.32	0.86	-0.036
D3	0.65	0.62	-0.033

4.3 Comments and discussions

This leeward edge definition introduced above can be a good approach to easily extract the leeward edge of the PJIC. Moreover, the fitting method allows the leeward edge to be mathematical expressed, which

can contribute to the establishment of an semi-empirical equation for the leeward edge.

However, there are a few uncertainties that should be addressed. Firstly, the extraction of the leeward edge is subject to the threshold value in the vertical vertical profile (0.25 maximum in this study), which suggests that the performance of this approach can be highly affected by the threshold selection. Therefore, it will be helpful to compare the variation of the leeward edge between different threshold. Secondly, this approach is highly dependent on the accuracy of the measurement technology. In this study, PIV, a global measurement technique was used to achieve the leeward edge. Technically, other anemometry apparatus, e.g. hot-wire and LDV, can be also used. Therefore, a comparison between different techniques is expected to contribute to a further validation of this approach. Thirdly, this approach has been attempted only for the single jet and the dual jets configurations. It is worth investigating whether this approach can be used for the primary jet in the multiple jets configurations. In addition, it is worth noting again that all assumptions and based on 2D measurement and the impact of the 3D representation can be underestimated. Therefore, an analysis of the effects from the third velocity component is expected.

5. NOISE REDUCTION USING THE PLANAR JET

An example of the flow-induced noise reduction using the planar jet is reported, which utilises an optimised position based on the leeward edge definition.

5.1 Shelter Optimization

As mentioned earlier, tandem cylinders were adopted as the test object. Fig.15 illustrates the relative position of the cylinders that is referred to the leeward edge. a is the horizontal position of the centre between two cylinders, and b is the top height of the cylinders. In order to maximise the noise reduction, an optimisation of a and b has been carried out, which is described in the following.

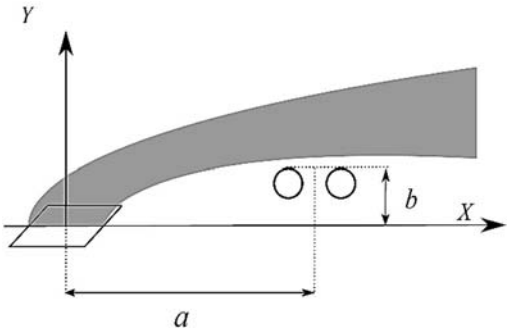

Fig. 15. Schematic of the tandem cylinders position.

It is known that the shelter to the tandem cylinders supplied by the planer jet dominates the performance of noise reduction. When a planar jet is used to reduce the flow-induced noise, it is expected to use the jet with the lowest speed to shelter the noise source. This is because the jet can generate substantial self-noise, i.e. jet noise (Tam 1998; Munro and Ahuja 2003). The self-noise intensity is positive correlated with the jet speed. The highest shelter of a jet stays below the peak of the leeward edge. Therefore, to use the jet with the lowest speed, it is reasonable to place the cylinders below the peak of the leeward edge so as to achieve maximum shelter height.

In this study, Case T1 in Tab.1 was applied to conduct the acoustic tests. To begin with, the leeward edge was fitted based on the PIV data. The experimental data, the fitted curve and the corresponding equation are depicted in Fig.16. Mathematically speaking, the peak of the leeward edge stays where the derivative of the polynomial equals to zero, i.e.d f (wx1)/d(wx1) = 0. The corresponding location is written in Fig.16, i.e. (7.82 w1,1.62 w1). Therefore, as discussed earlier, a was set to be equal to 7.82 w1, i.e. 78.2mm. This allows the horizontal position of the tandem cylinder to align with the peak of the jet leeward edge. As for b, it is obvious that b ≤ 1.62 w1. Considering the curvature of the leeward edge, a whole number was used and in the subsequent test and b was made to be 16mm.

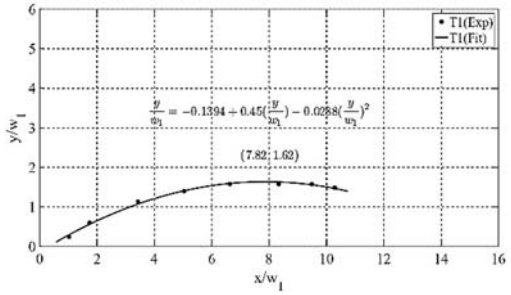

Fig. 16. Fitting of the leeward edge (T1).

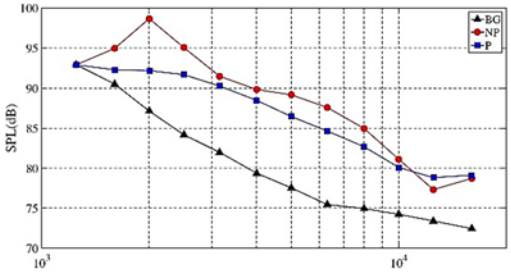

Fig. 17. One third octave band spectra related to the use of planar jet for flow induced noise reduction.

5.2 Acoustic Performance

In the acoustic experiment, three configurations were tested related to noise reduction, termed as BG, NP and P. In BG the cylinders were removed and the planar jet was turned off. This configuration was carried out to measure the background noise, e.g. power noise from the wind tunnel. In NP, the cylinders were installed. This configuration aimed to

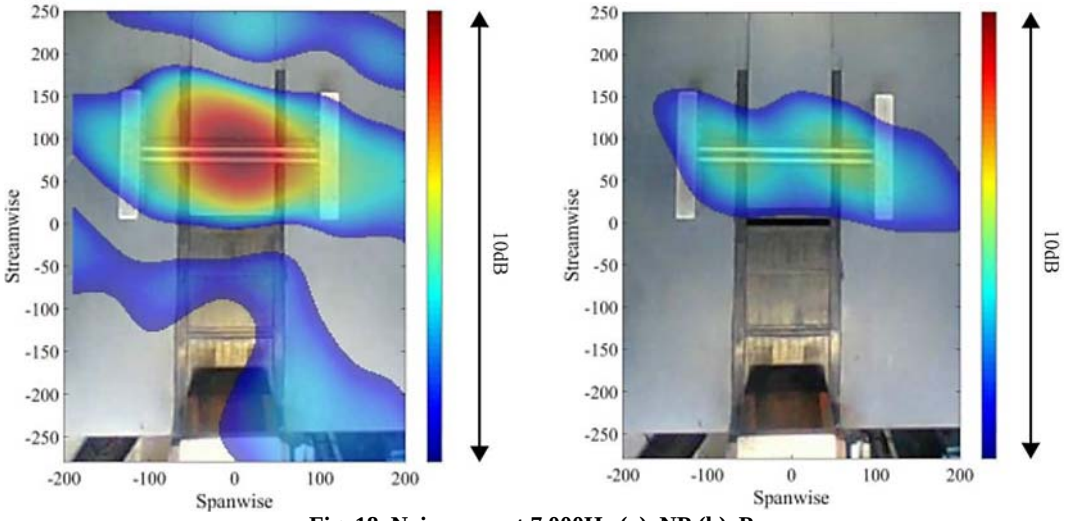

Fig. 18. Noise map at 7,000Hz (a). NP (b). P.

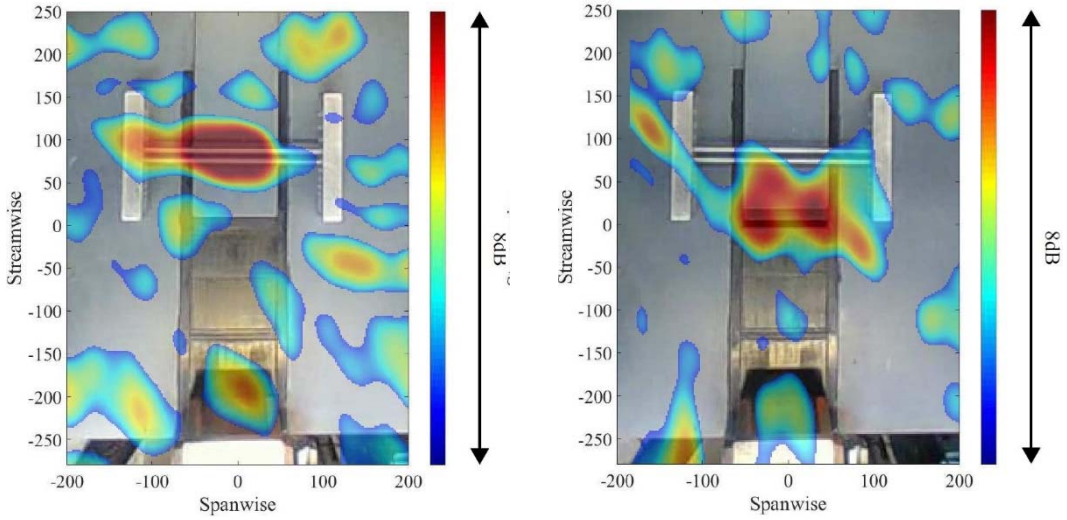

Fig. 19. Noise map at 14,000Hz (a). NP (b). P.

characterise the tandem cylinders noise. Note that in BG and NP, since there was no planar jet, the nozzle of the planar jet was removed and the outlet of the planar had been sealed. This is because when blown by the crossflow, the empty nozzle of the planar jet can act as a cavity and generate substantial cavity noise. In P, the planar jet was turned on to validate the noise reduction.

Fig.17 shows the overall one third octave band spectra of BG, NP and P in logarithm scale. In NP, it is obvious that SPL is much higher than BG, which means that the tandem cylinders can induce substantial noise. Moreover, a main tone can be found at 2,000Hz. This should correspond to the vortex shedding that occurs in the downstream field of the cylinders. When the planar jet is turned on in P, the spectrum comparison between NP and P shows that the cylinder noise can be significantly reduced. In particular, the tone discussed above has been well removed. More specifically, in the frequency of 2,000Hz, SPL can be reduced by 6.2dB, from 98.5dB to 92.3dB. Therefore, it is concluded that the planar jet can be of good use to reduce the flow-induced noise. More importantly, it is validated that the position optimisation can be based on the leeward edge definition approach in this study.

However, it is also found that SPL of P is still much higher than BG, which means that there are some subsequent noise sources after the planar jet is turned on. Moreover, it is found that in the bands between 11,220Hz and 17,780Hz, SPL of P is higher than NP, which means the introduction of the planar jet can make more noise than without the planar jet in these bands. In order to localise these subsequent noise source and explain the unexpected noise increase, the noise maps of NP and P are shown in Fig.18 and Fig.19, which corresponds to 7,000Hz and 14,000Hz respectively. The background image shows the picture taken by the array camera mentioned above. From the reader's view, the cylinders, the mass blocks, the wind tunnel nozzle and the test platform can be clearly observed. Note that as mentioned

earlier, the nozzle of the planar jet had been closed in NP, therefore, the out-let of the planar jet can be only found in the noise map of P. The coloured contour describes the SPL distribution within the beamforming measurement plane. Because of the dynamic range difference, the colour bar scale was set to be 10dB for Fig.18 and 8dB for Fig.19 to highlight the main noise source at different frequencies.

The noise maps of NP in both frequencies clearly illustrate that SPL is centred at the middle of the cylinders. This is where the vortex shedding mainly occurs. Therefore, the noise maps are in agreement with the spectra. When the planar jet is turned on, it is observed in Fig.18.b that at 7,000Hz the SPL is significantly reduced. The noise production is still centred at the cylinders, however, not in the middle but the side. This suggests that the subsequent noise generation may depend on the curvature of the crossflow deflected by the planar jet. By contrast, Fig. 19.b shows that the subsequent main noise source is displaced from the cylinders to the outlet of the planar jet. It appears that no reduction is achieved at 14,000Hz. This suggests that the planar jet self-noise has become another subsequent main noise source. As such, the SPL increase in the bands between 11,220Hz and 17,780Hz, can be attributed to the jet self-noise.

5.3 Discussions

In this section, with the position achieved from the leeward edge definition approach described in this study, the use of the planar jet towards the flow induced-noise reduction has been discussed. It is found that despite significant noise reduction, the cylinders and the planar jet can be the subsequent main noise source in different frequency ranges respectively. In particular, in the high frequency range, the jet self-noise substantially contributes to the total noise emission and SPL can be higher than without the planar jet. Therefore, this self-noise may impede the implementation of the planarjet, which necessitates the self-noise suppression. Moreover, the leeward edge definition has been validated to be able to find an optimised shelter to the tandem cylinders. Therefore, due to the usefulness of this approach, further investigations, especially with more parametric analysis on this approach, are expected.

6. CONCLUSIONS

In this paper, a novel approach to defining the leeward edge of the planar jet in crossflow was introduced. The approach was validated for the single jet and the dual jets configurations in crossflow. The application of this approach on the flow induced-noise was discussed. In addition, the algorithm of the PIV frame assembly was reported.

To define the leeward edge, the PIV assembly was carried out to capture the jet development in the crossflow. Based on the PIV data, the approach adopted a threshold to distinguish those regions that are sheltered and not sheltered by the planar jet in each velocity profile. Therefore, the locus of those threshold points was defined as the leeward edge. Furthermore, it is validated that the second order polynomial is able to fit the leeward edge of the primary jet in the single jet and the dual jets configurations. This fitting allows the leeward edge to be mathematically expressed. The usefulness of this approach was subsequently confirmed by an application for the flow-induced noise reduction. The shelter position aligning with the leeward edge peak was found using the approach. The acoustic tests showed that the flow induced noise of the tandem cylinders at the shelter position can be significantly reduced. Moreover, it is foreseen that a semi-empirical equation of the leeward edge can be achieved based on the mathematical expression in this approach.

REFERENCES

Ahmed, K., D. Forliti, J. Moody and R. Yamanaka (2008). Flowfield characteristics of a confined transverse slot jet. *AIAA journal 46*(1), 94–103.

Amiet, R. (1978). Refraction of sound by a shear layer. *Journal of Sound and Vibration 58*(4), 467–482.

Bennett, G. J., K. Zhao, J. Philo, Y. Guan and S. C. Morris (2016). Cavity noise suppression using fluidic spoilers. In 22nd *AIAA/CEAS Aeroacoustics Conference*, Lyon, France.

Camussi, R. (2002). Coherent structure identification from wavelet analysis of particle image velocimetry data. *Experiments in Fluids 32*(1), 76–86.

Camussi, R., G. Guj and A. Stella (2002). Experimental study of a jet in a crossflow at very low reynolds number. *Journal of fluid mechanics 454*, 113–144.

Haniu, H. and B. Ramaprian (1989). Studies on two-dimensional curved nonbuoyant jets in cross flow. *Journal of fluids engineering 111*(1), 78–86.

Jones, W. and M. Wille (1996). Large-eddy simulation of a plane jet in a cross-flow. *International journal of heat and fluid flow 17*(3), 296–306.

Koched, A., M. Pavageau and F. Aloui (2011). Vortex structure in the wall region of an impinging plane jet. *Journal of Applied Fluid Mechanics 4*(2 -s 1), 61–69.

Kotsovinos, N. E. (1976). A note on the spreading rate and virtual origin of a plane turbulent jet. *Journal of Fluid Mechanics 77*(02), 305–311.

Larsson, I., E. M. Lindmark, T. S. Lundström, B. Marjavaara and S. Töyrä (2012). Visualization of merging flow by usage of piv and cfd with application to gratekiln induration machines. *Journal of Applied Fluid Mechanics 5*(4), 81–89.

Lin, Y. and M. Sheu (1991). Interaction of parallel turbulent plane jets. *AIAA journal 29*(9), 1372–

1373.

Mahesh, K. (2013). The interaction of jets with crossflow. *Annual review of fluid mechanics 45*, 379–407.

Morton, B. R. and A. Ibbetson (1996). Jets deflected in a crossflow. *Experimental Thermal and Fluid Science 12*(2), 112–133.

Munro, S. E. and K. Ahuja (2003). *Aeroacoustics of a high aspect-ratio jet*. Hilton Head, SC, United states.

Oerlemans, S. and A. Bruin (2009). Reduction of landing gear noise using an air curtain. In 15th *AIAA/CEAS Aeroacoustics Conference*, Miami, Florida, USA.

Pavageau, M., K. Loubière and S. Gupta (2006). Automatic eduction and statistical analysis of coherent structures in the wall region of a confined plane turbulent impinging jet. *Experiments in Fluids 41*(1), 35–55.

Persen, L. N., H. iann and H. P. Mazumdar (1993). The round thermal jet: undisturbed and in cross-flow. *International Journal of Heat and Mass Transfer 36*(6), 1589 – 1599.

Rajaratnam, N. (1976). *The plane turbulent freejet. In Turbulent jets*. Elsevier.

Ramaprian, B. and M. Chandrasekhara (1985). Lda measurements in plane turbulent jets. *Journal of Fluids Engineering 107*(2), 264–271.

Rudman, M. (1996). Simulation of the near field of a jet in a cross flow. *Experimental Thermal and Fluid Science 12*(2), 134–141.

Sijpkes, T. and J. Wickerhoff (2004). *Aeroplane provided with boise-reducing means, as well as a landing gear and blowing means.* US Patent US20040104301 A1.

Smith, S. and M. Mungal (1998). Mixing, structure and scaling of the jet in crossflow. *Journal of fluid mechanics 357*, 83–122.

Tam, C. K. (1998). Jet noise: since 1952. *Theoretical and Computational Fluid Dynamics 10*(1-4), 393–405.

Tanaka, E. (1974). The interference of two-dimensional parallel jets: 2nd report, experiments on the combined flow of dual jet. *Bulletin of JSME 17*(109), 920–927.

Yu, D., M. S. Ali and J. H. W. Lee. Multiple tandem jets in cross-flow. 132(9), 971–982.

Zdravkovich, M. (1985). Flow induced oscillations of two interfering circular cylinders. *Journal of Sound and Vibration 101*(4), 511–521.

Zdravkovich, M. (1987). The effects of interference between circular cylinders in cross flow. *Journal of fluids and structures 1*(2), 239–261.

Zhao, K., P. N. Okolo, J. Kennedy and G. J. Bennett (2016). A study of planar jet flow control and perforated fairings for the reduction of the flow-induced noise of tandem rods in a cross-flow. In *22nd AIAA/CEAS Aeroacoustics Conference*, Lyon, France, 2772.

Zhao, K., X. Yang, P. N. Okolo, Z. Wu and G. J. Bennett (2017). Use of dual planar jets for the reduction of flow-induced noise. *AIP Advances 7*(2), 025312.

Zhao, K., X. Yang, P. Okolo and W. Zhang (2016). Use of a plane jet for flow-induced noise reduction of tandem rods. *Chinese Physics B 25*(6), 64301.